Experimental study of transverse effects in planar dielectric wakefield accelerating structures with elliptical beams

Y. Saveliev,[1,2] T. J. Overton,[2,3] T. H. Pacey,[1,2,*] N. Joshi,[1,2] S. Mathisen,[1,2] B. D. Muratori,[1,2] N. Thompson,[1,2] M. P. King,[1,2] and G. Xia[2,3]

[1]*ASTeC, STFC Daresbury Laboratory, Warrington, WA4 4AD, United Kingdom*
[2]*Cockcroft Institute, Daresbury, Warrington, WA4 4AD, United Kingdom*
[3]*The University of Manchester, Manchester, M13 9PL, United Kingdom*

(Received 6 April 2022; revised 7 July 2022; accepted 9 August 2022; published 24 August 2022)

The main obstacle to the practical implementation of the dielectric wakefield acceleration (DWA) concept is the development of the beam breakup instability due to transverse dipole wakefields generated when the beam propagates off axis in the accelerating structure. One of the methods to suppress this instability is to elliptically shape the beam and accelerate it in a planar structure. Here, we report a detailed experimental investigation of the transverse dynamics of elliptical beams in planar dielectric structure with parameters mimicking future DWA modules. Both dipole and quadrupole wakefields' effects on beam stability and projected emittance were studied. This study has highlighted the importance of counteracting quadrupole wakefields in future DWA implementations.

DOI: 10.1103/PhysRevAccelBeams.25.081302

I. INTRODUCTION

Dielectric wakefield acceleration (DWA) is one of the novel acceleration concepts that has been actively developed in recent years as a technology for future linear colliders and free-electron lasers, offering higher accelerating gradients and lower costs in comparison to "classic" rf accelerators. Accelerating gradients in the GV/m range have been recently demonstrated experimentally [1]. Metal corrugated structures with a similar underlying physical mechanism have been also considered [2–4].

The collinear DWA concept is based on a high charge drive electron bunch generating a large wakefield that accelerates a trailing main bunch in the same dielectric channel. Apart from high accelerating gradients, practical and efficient DWAs must also ensure a high transformer ratio (TR): the ratio of the maximal accelerating field for the main bunch and the maximal decelerating field of the drive bunch. Theoretical studies demonstrated that to achieve both, the accelerating gradients are limited to several 100s of MV/m level [5] by the necessity to shape the drive bunch longitudinal profile as triangular, double-triangular, or "door-stop" [6,7] with an unavoidable increase of the bunch length to ps range.

The major obstacle to the practical implementation of the DWA concept is the beam breakup (BBU) instability that develops if the beam propagates off axis in the DWA structure. A widely accepted concept for BBU suppression is Balakin, Novokhatski, Smirnov (BNS) damping [8] explored theoretically [9,10] which is currently the basis for prototype DWA modules [11]. Although the BNS damping is shown to significantly suppress the development of the BBU instability, it may still not be sufficient for long (tens of meters) accelerating channels and imposes very strong requirements on manufacturing and alignment tolerances of the quadrupole wiggler around DWA down to micrometer level [9,12].

An alternative method could be the implementation of planar DWA structures with elliptical, high aspect ratio, beams due to the reduction of the coupling to the transverse wakefield modes that was theoretically demonstrated in a number of studies [13–15]. Planar wakefield structures have been experimentally investigated extensively with emphasis on the longitudinal beam dynamics [16–19] or generation of THz Cerenkov radiation [4,20] but transverse effects were studied to a lesser extent [21,22].

The first and, to the best of our knowledge, the only experimental investigation of transverse effects in planar DWA structures with elliptical beams was reported in [23]. These experiments were conducted at FACET (SLAC National Accelerator Laboratory) using 20.35-GeV electron beams with a high bunch charge of 3.2 nC. The DWA structures were, however, 10 mm long, with a small gap of less than 1 mm, and beam position monitors (BPMs) were used to observe transverse effects. These limitations prevented simultaneous measurements of longitudinal fields

*thomas.pacey@stfc.ac.uk

and transverse fields that were measured only in terms of c.m. (center of mass) variation.

In this article, we present the results of a study on transverse effects in planar DWA structures with elliptical electron beams at 35-MeV energy. This lower energy and the use of screens for beam imaging, rather than BPMs, allowed us to observe not only transverse dipole fields but also transverse quadrupole and longitudinal ones even at low bunch charges of 85–100 pC.

II. EXPERIMENTAL SETUP

Experiments were conducted in Beam Area 1 (BA1) of the CLARA facility [24] at Daresbury Laboratory. BA1 features a 2-m long vacuum chamber which enables the study of DWA structures with lengths and gaps similar to modules of future accelerators. In these experiments, the structure was identical to that designed originally for the energy dechirper at CLARA [25,26]: 200 mm long in the z direction, and 10 mm wide in the x direction with quartz plates of 200 μm thickness (see Fig. 1 for the coordinate system). It was mounted on a translation stage to vary the beam offset from the structure axis in the vertical direction and the structure gap could be also varied with an additional stage in the vertical y direction. Due to the variation of both structure gap and beam offset, the frequency of the fundamental longitudinal section magnetic (LSM) mode and overall wakefield spectrum content was also changed in the experiment. To illustrate, for $a = 0.5$ mm, the $\mathrm{LSM}_{1,1}$ mode has a frequency of 143 GHz and reduces to 113 GHz at $a = 1.0$ mm. The next higher order modes ($\mathrm{LSM}_{2,m}$) have frequencies of the order 500 GHz. The overall design provided a possibility to remotely adjust the tilt of the structure with respect to the electron beam.

A schematic of the CLARA BA1 layout is shown in Fig. 1. The upstream quadrupole triplet Q1 focuses the beam to the desired size at the screen S3 positioned in the middle of the 200-mm long DWA structure. The downstream triplet Q2 manipulates the beam size and the beam optical function β_x on the energy spectrometer screen S6. A single quadrupole Q3 was used to control horizontal dispersion at the S6 position. In these experiments, the dispersion was varied in the range of 460–1200 mm to accommodate different widths of energy spectra. Horizontal and vertical scanning slits for emittance measurements, each with 50 μm width, were positioned 0.50 m from the DWA center.

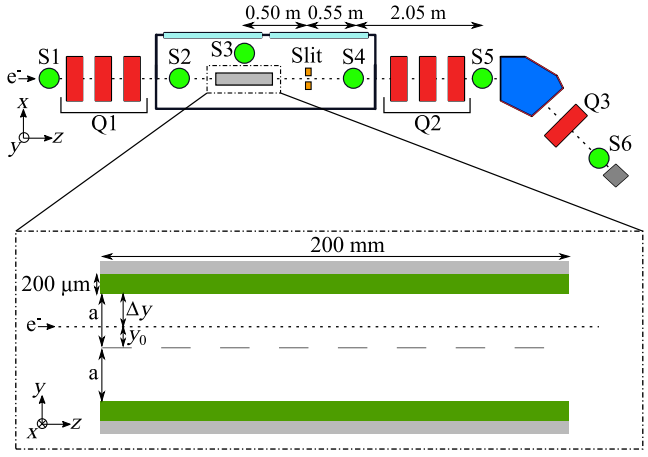

FIG. 1. Schematic of the experiment performed at CLARA BA1, with an inset showing the DWA structure and coordinate system used for defining structure gaps and beam offsets.

The majority of measurements were made with a bunch charge of 85 pC; however, this could not be always maintained consistently during machine operation. Some results were therefore scaled to 85 pC since the wakefield strengths are proportional to bunch charge [27]. During measurements, care was taken to ensure full beam transmission through the structure by choosing the appropriate range of structure gaps and beam offsets. The bunch length could be easily varied from the CLARA facility by varying the accelerating off-crest phase in the linac [24]. To minimize the variation of the transverse beam optics at different linac off-crest phases, the beam energy was maintained at nominal 35 MeV by adjusting the linac gradient. For these experiments, we have chosen a relatively long bunch length of 800 fs rms that is more representative of bunch lengths required for achieving high transformer ratios with triangular, double-triangular, or door-stop longitudinal bunch profiles [6,12,19]. Some data were also collected with shorter, 300-fs bunches for comparison and in part for benchmarking the simulations. Bunch lengths were measured by a wakefield streaking method [28] and corroborated by electro-optic measurements. While the horizontal beam size (x direction in Fig. 1) in the DWA structure was varied over a wide range of up to 1500 μm rms, the vertical size (y direction in Fig. 1) of 150 ± 20 μm was kept approximately constant. This relatively large vertical beam size was chosen to minimize the beam envelope variation within the long DWA structure and to ensure small beam sizes on downstream screens.

III. SIMULATION METHODOLOGY

The experimental results are compared with the simulations that follow the methodology described in [29]. This method provides the 3D Green's functions for a given planar DWA structure through decomposition into discrete transverse modes. The resulting functions are then convolved with a macroparticle distribution that has been distributed onto a discrete mesh grid. This allows modeling of the resulting 3D wakefield from electron bunches with arbitrary transverse and longitudinal distributions, with no constraints on symmetry. In contrast to electromagnetic finite difference time domain (EM-FDTD) solvers for Maxwell's equations, this method requires the simulation domain to only cover the volume described by the electron

beam and not the whole transverse DWA geometry. This implementation has reduced the time for simulations by orders of magnitude, thus eliminating the need for a high performance computing cluster. The simulations can be performed with modest computer resources, even when a large number of modes are needed for accurate results. The number of modes is set for each calculation to ensure convergence of the final field, ensuring the accuracy of the simulation across varying bunch and structure parameters. The wakefields calculated by the code have been benchmarked against commercial EM-FDTD software packages CST and VSim, with consistent results obtained.

IV. RESULTS

Typical images of the 800-fs long bunch on the screen S5 (while the quadrupole triplet Q2 is switched off) at different beam offsets y_0 in the DWA structure, see Fig. 1, with the gap set to $2a = 4.0$ mm are shown in Fig. 2.

It is evident that the vertical beam size increases while the beam is set to smaller distance Δy from the dielectric plate due to increasing vertical dipole wakefield F_y. Two vertical image profiles are shown in Fig. 2 for $y_0 = 0$ (beam set to the axis of the structure) and 1.54 mm. Apart from dipole wakefields, the planar dielectric structure exhibits strong quadrupole-like wakefields even with the beam on the structure axis. The vertical quadrupole field is defocusing thus contributing to the size of the streaked image and reducing the resolution of a resulting bunch longitudinal profile reconstruction [30]. The strength of F_y along this long 800-fs bunch is highly nonlinear and "flattens" toward its tail—as shown in Fig. 3—resulting in a small "hump" evident in the vertical profile. With F_y being nearly constant at the tail of the bunch, a larger portion of the charge from adjacent longitudinal slices is projected onto the screen at approximately the same vertical position.

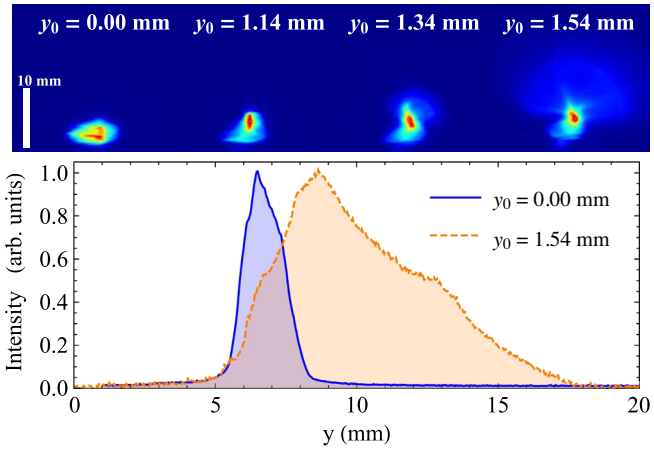

FIG. 2. Top: Beam images on the S5 screen at various offsets in the structure with the half-gap of $a = 2.0$ mm. The bunch length is 800 fs and the rms horizontal beam size $\sigma_{x0} = 360$ μm. Bottom: vertical projections at $y_0 = 0$ and 1.54 mm.

In the horizontal plane, the behavior is more complicated due to the focusing nature of the quadrupole field. Longitudinal beam slices near the head of the bunch experience net focusing while the following slices are first focused into the waist and then become strongly overfocused toward the tail.

The complex behavior of the quadrupole-like wakefield F_x is also evident when the beam width σ_{x0} and structure gap are varied. Figure 4(a) shows horizontal divergence calculated as $\sigma' = (\sigma_{S5} - \sigma_{S4})/L$ where σ_{S4} and σ_{S5} are rms beam sizes on screens S4 and S5 and $L = 2.05$ m is the distance between them. The dotted black line represents the beam divergence when the structure is withdrawn. Strictly speaking, data presented in Fig. 4(a) can be interpreted as divergence only if the beam waist is upstream of the S4 screen located 1.05 m from the middle of the structure. For the smallest gap of $a = 0.5$ mm, this is valid for $\sigma_{x0} <$ 800 μm where strong horizontal focusing takes place even for these relatively wide beams. The increase in the beam width significantly reduces horizontal focusing. With larger half-gaps of 0.75 and 1.0 mm, the focusing is significantly weaker; however, the effect of the beam width is also diminished.

In the vertical plane, the interpretation of experimental data presented in Fig. 4(b) is more straightforward because the vertical defocusing field is increasing the natural divergence of the beam. Similar to the horizontal plane, defocusing is greatly reduced with increased structure gaps and diminishes with increased beam width.

Although it is not straightforward to interpret experimental measurements in Fig. 4, corresponding simulations corroborate the data. Both indicate that the horizontal focusing kick is within the range of 0.2–0.3 mrad, even

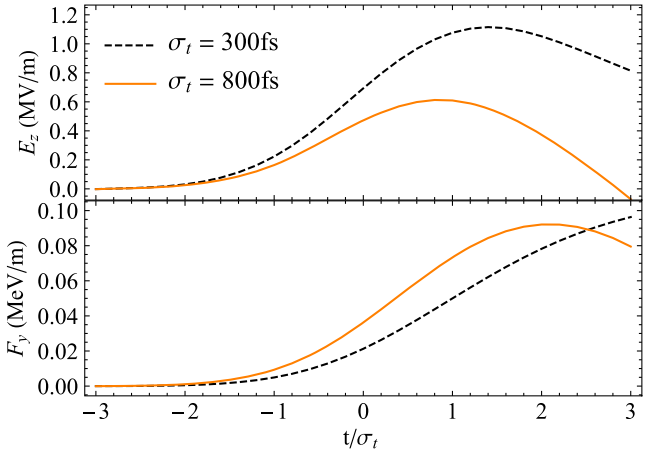

FIG. 3. Comparison of simulated longitudinal E_z (top) and vertical F_y (bottom) wakefields for an 85-pC Gaussian bunch with lengths $\sigma_t = 800$ and 300 fs, and $\sigma_x = \sigma_y = 150$ μm. The longitudinal coordinate is normalized to the bunch σ_t and the F_y field is plotted at $y = 2\sigma_y = 300$ μm. The DWA structure half-gap is $a = 1$ mm.

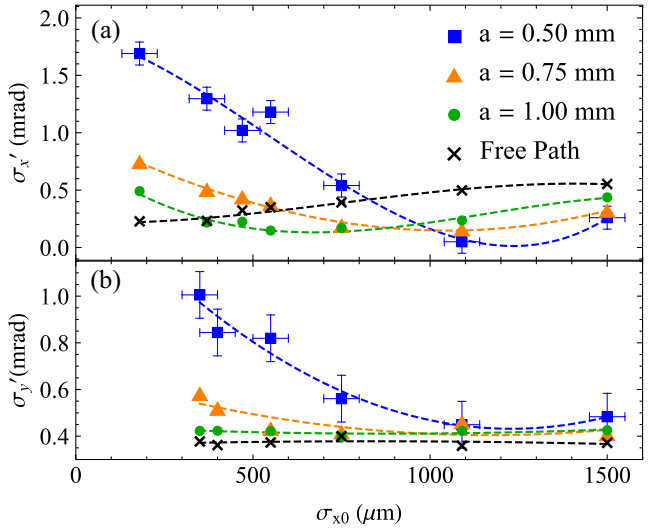

FIG. 4. Beam divergence calculated as $\sigma' = (\sigma_{S5} - \sigma_{S4})/L$ where $L = 2.05$ m is the distance between screens in horizontal (a) and vertical (b) planes. Dashed lines are third order polynomial fits to aid legibility. Measurements are presented for structure half-gaps of $a = 0.5$, 0.75, and 1.0 mm. The beam is set on axis of the structure at each gap and the bunch length is $\sigma_t = 800$ fs. Error bars shown for $a = 0.5$ mm data are representative of errors for other half-gaps, which are omitted to aid legibility.

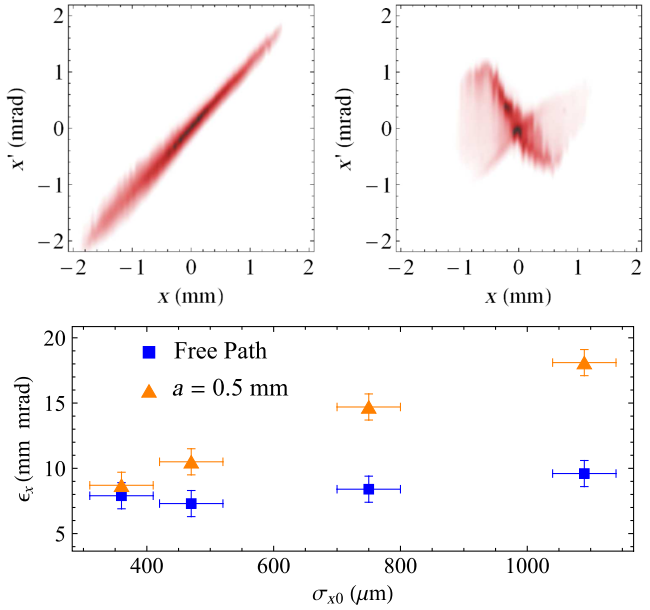

FIG. 5. Top: horizontal phase spaces of the beam with $\sigma_{x0} = 0.75$ mm propagating in the free path (left) and through the structure set to $a = 0.5$ mm (right). Bottom: dependence of the horizontal projected emittance on beam size σ_{x0}.

at $\sigma_{x0} > 500$ μm. This may have important implications for the practical design of the planar DWA modules with elliptical nC scale drive bunches. Transverse dynamics of an elliptical beam with a bunch charge of 10 nC were studied through simulation and the results are presented in Sec. V.

An example of the horizontal phase space with and without DWA structure with the half-gap of $a = 0.5$ mm reconstructed from slit scans is given in Fig. 5 for the case of $\sigma_{x0} = 750$ μm. The focusing quadrupole wakefield F_x is strong enough to transform the main body of the beam from being divergent to convergent. The transverse phase space also shows that F_x is not linear across this wide beam and reduces toward its edges. The projected emittance is higher compared to that measured with the beam propagating in the free path. The dependence of the projected emittance on transverse beam size σ_{x0} calculated from slit scans is also shown in Fig. 5. As expected from simulations, the horizontal emittance increases with an increase in the beam size. The emittance in the vertical plane was also measured but a large variance of measurement—due to the small vertical beam size at the slit position—did not allow making a reliable conclusion.

To demonstrate the feasibility of the BBU suppression in planar DWA structures with elliptical beams, the beam should be offset from the structure axis and variation of both F_y and E_z should be measured as a function of the beam size σ_{x0} at the structure. In order to be representative of a practical (nC scale) DWA, we used a larger structure gap of $2a = 4.0$ mm and correspondingly larger offsets to emphasize those transverse effects.

Suppression of BBU with elliptical beams in planar DWA structures relies on theoretical predictions [13,14] that transverse wakefields are reduced at a much greater rate, $1/\sigma_x^3$, compared to longitudinal ones, $1/\sigma_x$. This difference was observed experimentally as demonstrated in Fig. 6 where the average decelerating field E_z and vertical dipole field F_y are given as a function of the horizontal beam size σ_{x0} for two different quasi-Gaussian rms bunch lengths of 800 and 300 fs. The experimental values of F_y were calculated from the c.m. change of beam images in the vertical plane on downstream screens S4 and S5 with and without the structure. At larger structure gaps and larger beam offsets, the wakefields depend primarily on the distance Δy between the beam centroid and the dielectric plate rather than the structure half-gap a. The data are therefore presented without normalization of σ_{x0} to a. As expected, the average longitudinal field E_z was found to be approximately 2 times stronger with shorter bunches, while the transverse field F_y was approximately the same level compared to 800-fs bunches. Limitations of the accuracy of our measurement of average F_y prevent differentiation between two measured cases. Lines in Fig. 6 are simulations of the experiment conditions and these match the measured data very closely for E_z. The data match the simulated trend for F_y, even if the small change predicted by simulations was not observed. Note that the simulated averaged F_y values are slightly smaller with the

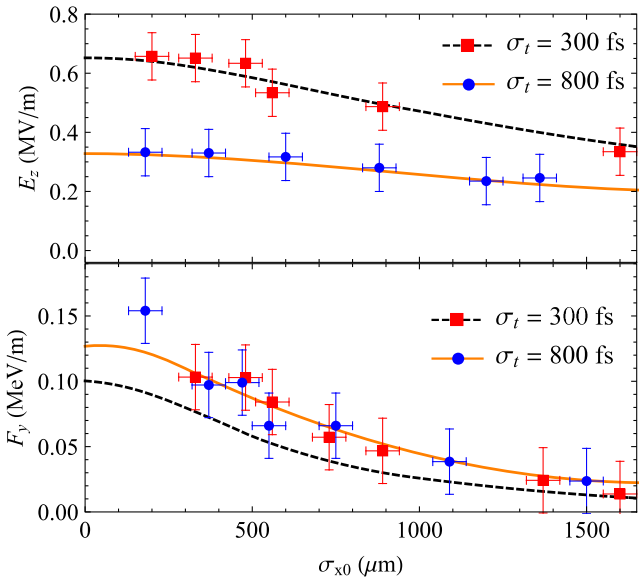

FIG. 6. Average longitudinal E_z and transverse F_y wakefield strengths as a function of the rms beam size at the position of the DLW. E_z is measured with the structure half-gap of $a = 1.0$ mm and beam centered. F_y is measured with $a = 2.0$ mm and $y_0 = 1.34$ mm. rms bunch lengths of $\sigma_t = 800$ and 300 fs were used. The lines are corresponding simulation results.

shorter 300-fs bunch length. At a given bunch charge (identical for both bunch lengths), the peak of the transverse wakefields is indeed larger for a shorter bunch but this peak is located well behind the 300-fs bunch. At 800 fs, on contrary, the field peaks at the tail of the bunch and affects a larger portion of the total charge, as shown in Fig. 3. Hence the average values of F_y—across the whole bunch—are similar or even somewhat smaller for a shorter bunch.

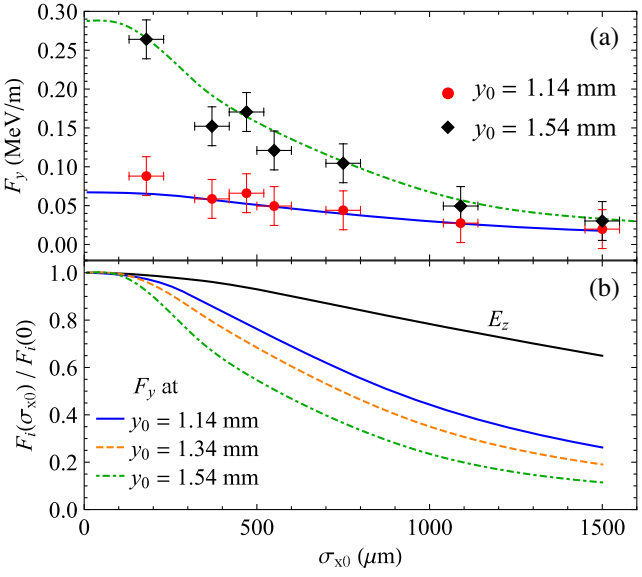

FIG. 7. (a) Average transverse F_y wakefield strengths as a function of σ_{x0}. F_y is measured with a structure half-gap of $a = 2.0$ mm, and offsets $y_0 = 1.14$ and 1.54 mm. rms bunch length is set to 800 fs. Lines—corresponding simulation results. (b) Normalized simulated dependencies of E_z and F_y on σ_{x0} from Figs. 6 and 7(a).

Average dipole fields F_y for two further offsets and a bunch length of 800 fs are given in Fig. 7(a). Lines represent simulated results with, again, a good match to experimental data. All simulated curves are also combined together in Fig. 7(b) and presented in a normalized form. Normalization is made to the highest value of F_y at $\sigma_{x0} = 0$ for a given offset. For beams with large transverse ellipticity, coupling to higher order transverse modes is reduced [14]. These higher order modes contribute to transverse fields to a greater extent than longitudinal fields. Indeed, F_y falls off much faster than E_z with increasing σ_{x0}, especially at larger offsets y_0 (smaller distances to the plate).

V. SCALING TO HIGH CHARGE, HIGH ENERGY ACCELERATOR

Although elliptical high aspect ratio electron beams in planar structures reduce the transverse dipole wakefields that cause the development of the BBU instability, the effects of quadrupole wakefields have to be taken into consideration while evaluating the feasibility of this acceleration scheme. In this section, we describe the results of simulations performed with high charge drive bunches propagating through a long planar structure.

We consider bunches with charge $Q = 10$ nC, 1 GeV beam energy and skew Gaussian longitudinal profile,

$$\rho(t) = \frac{Q}{\sqrt{2\pi}\sigma_t}\,\mathrm{erf}\left(\frac{-\alpha t}{\sqrt{2}\sigma_t}\right)\exp\left(-\frac{t^2}{2\sigma_t^2}\right),$$

rms bunch length, $\sigma_t = 1$ ps, and skew factor $\alpha = -4$. This profile is shown in Fig. 8(a) and approximates a triangular profile similar to those considered for future wakefield accelerators. The total bunch length is 3 ps, with peak current ≈7 kA, the vertical beam size $\sigma_{y0} = 50$ μm, and the horizontal beam size $\sigma_{x0} = 500$ μm (using the coordinate system shown in Fig. 1). The projected normalized emittance was set to a low value of 0.05 μm to eliminate effects from the beam envelope development and demonstrate only wakefield effects. The planar structure gap was set to $2a =$ 2.0 mm which is representative for practical wakefield accelerators [31]. For reference, Fig. 8(b) shows also transverse wakefield forces F_x and F_y along the bunch calculated at coordinates (x, y) of $(2\sigma_x, 0)$ and $(0, 2\sigma_y)$, respectively.

As noted in Sec. IV, the beam behavior in the horizontal plane is complex owing to the variation of F_x transversely and longitudinally. To illustrate this behavior, the bunch was divided into five identical longitudinal slices of 0.4 ps each as shown in Fig. 8(a). Summarily, these slices

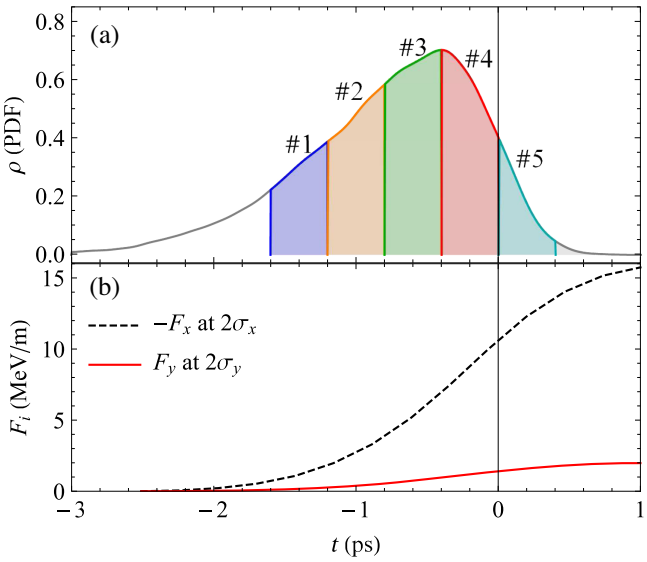

FIG. 8. (a) Skew Gaussian longitudinal bunch profile used in simulations at 1 GeV and 10 nC. Five longitudinal slices of 0.4 ps width each that were studied individually are also shown. (b) Transverse wakefield forces along the bunch on the structure axis. Horizontal F_x is calculated at coordinates $(x, y) = (2\sigma_x, 0)$ and vertical F_y at $(x, y) = (0, 2\sigma_y)$, where $\sigma_x = 500$ μm and $\sigma_y = 50$ μm.

represent 8.9 pC of the total 10 pC bunch charge. Horizontal rms widths σ_x of longitudinal slices along the 5 m length of the structure are given in Figs. 9(a) and 9(b). Here, the vertical wakefields were deliberately removed by setting $F_y = 0$ to isolate only the horizontal effects from F_x. Note also that 95% of macroparticles were used to calculate σ_x values to remove the contribution of outlier particles with excessive offsets.

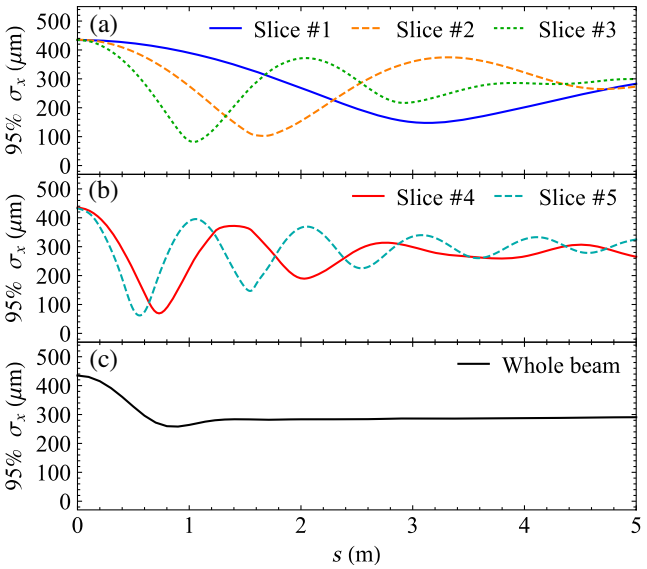

FIG. 9. Variation of horizontal rms beam sizes along the DWA structure. Initial beam size is $\sigma_{x0} = 500$ μm but 5% of particles with largest deviation from the axis are discounted. The beam is set on axis. Vertical wakefields F_y are removed. (a, b) five slices as shown in Fig. 8. (c) projected size of the whole beam.

Each slice exhibits oscillatory behavior with the frequency of oscillations increasing toward the tail of the bunch in accordance with longitudinally increasing F_x. The amplitude of oscillations is rapidly decaying, with a corresponding variation in oscillation frequency, as a result of F_x variation within the relatively thick longitudinal slices. With sufficient propagation, each slice tends to reach a steady state with $\sigma_x \approx 300$ μm. It should be noted that even for very thin longitudinal slices—which do not have an appreciable variation of F_x along the slice—these quasi-betatron oscillations also decay, albeit much slower. This effect within a thin slice is caused by a different underlying mechanism: the transverse nonlinearity of $F_x(x)$ across a wide electron beam which increases at larger σ_{x0}. This was evident from particle tracking in the transverse phase space. All of the above results in the projected horizontal beam size reaching a steady state with negligible oscillations, see Fig. 9(c).

Even though the rms beam size σ_x reduces by a relatively small amount of ≈30%, the transverse horizontal profile undergoes a significant transformation as evident in Fig. 10. From an initially Gaussian distribution, a strong peak develops at the beam center after ≈1 m of propagation through the structure and this profile remains largely unchanged afterward. Such a profile will have a reduced effect on the suppression of transverse wakefields, including the dipole component of the F_y, if compared to the initial 500-μm Gaussian distribution.

Transverse quadrupole wakefields significantly disrupt beam propagation through the structure causing the onset of beam losses after ≈1 m even with the beam set on axis as seen in Fig. 11. This plot shows also the dependence of beam losses with distance when the horizontal force F_x is removed (dotted line) to emphasize the effect of horizontal profile variation. Particle distributions in y-t plane are also shown at the start of the structure in Fig. 12(a) and after 1.5

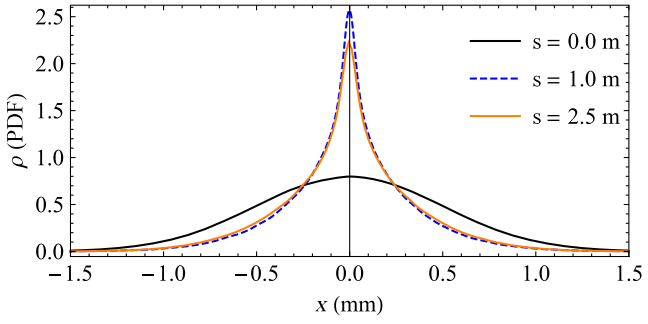

FIG. 10. Horizontal beam profiles at $s = 0$ (initial) and at $s =$ 1.0 and 2.5 m. The beam is set on axis and vertical wakefields F_y removed.

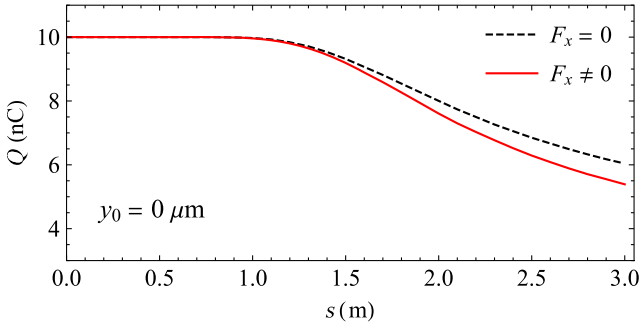

FIG. 11. Bunch charge as a function of propagation distance through the structure. Plots are shown for F_x removed (dotted line) and included (solid line). The beam is on the structure axis.

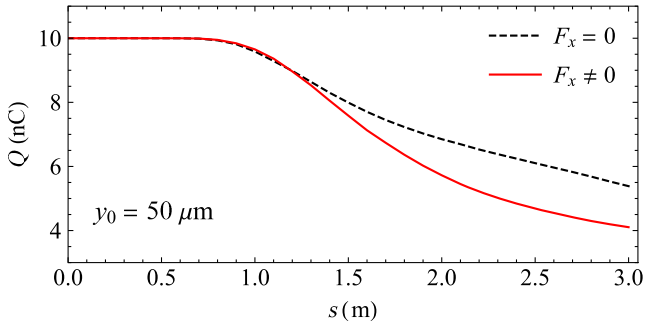

FIG. 13. Bunch charge as a function of propagation distance through the structure with the beam offset vertically by $y_0 = 50\ \mu$m. Plots are shown for F_x removed (dotted line) and included (solid line).

and 2.5 m of propagation in Figs. 12(b) and 12(c). The beam losses, and the difference between cases with and without F_x, increase when the beam is initially offset vertically by 50 μm, see Fig. 13. BBU instability development is evident in the particle distributions shown in Fig. 14.

The bunch has lost more than half of its charge after only 3 m of propagation. At this point, slices 4 and 5 (indicated in Fig. 8) have been eroded, only ≈10% of the charge in slice 3 remains, and losses in slice 2 have started, see Fig. 15. Since the lost slices are positioned at the tail of the bunch, the longitudinal bunch profile changes, and the effective bunch length is reduced as shown in Figs. 14(a) and 14(b). Therefore, in addition to a reduction of the longitudinal wakefield E_z due to diminished bunch charge, the transformer ratio has been impacted and reduced the accelerating gradient behind the drive bunch.

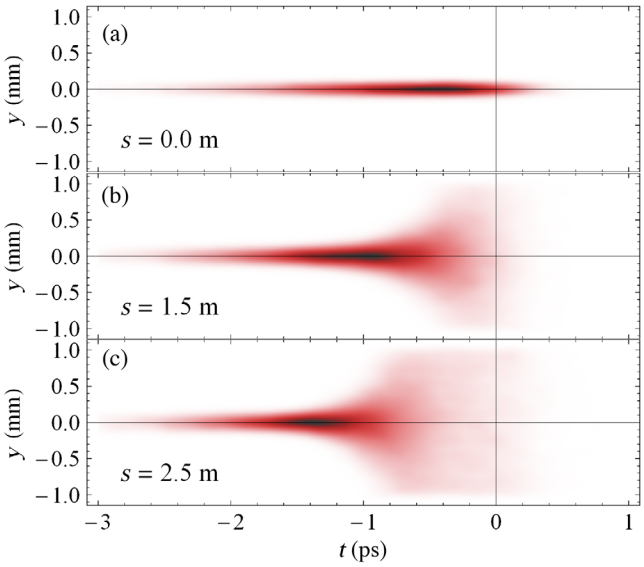

FIG. 12. Transverse-longitudinal distribution of particles after propagation distances of $s = 1.5$ and 2.5 m from the beginning of the structure ($s = 0$). The beam is on the structure axis. F_x is included.

One may conclude from these simulations that the simple concept of BBU suppression with elliptical beams in planar structures may not provide a scalable solution for DWAs as the quadrupole wakefields also need to be counteracted. One method to achieve this is well known and represents a sequence of short DWA sections with alternating orthogonal orientation [32] which has been implemented already for energy dechirpers in FELs [25,33,34]. The efficiency of this method was demonstrated by simulations in the case of a small size circular beam [35]. The application of this method to large aspect ratio elliptical beams is not straightforward. The main obstacle would be filling the aperture of every other structure with beam thus causing strong nonlinearities and excessively large wakefields at the beam edges. This represents a very complex problem that requires a dedicated study.

As evident from Fig. 14, the elliptical beam with $\sigma_{x0} = 500\ \mu$m is not able to suppress the BBU instability fully. Further increase in σ_{x0} would extend the length of propagation due to a further reduction in transverse wakefields strength (Fig. 7) but, in this case, compensation of

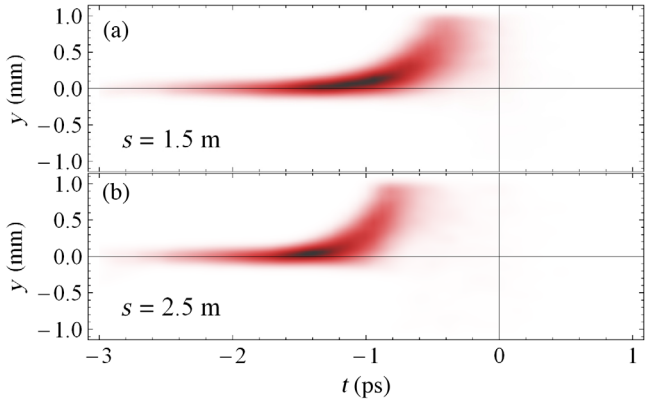

FIG. 14. Transverse-longitudinal distribution of particles after 1.5 and 2.5 m propagation distance through the structure. The beam is initially offset vertically by $y_0 = 50\ \mu$m. F_x is included.

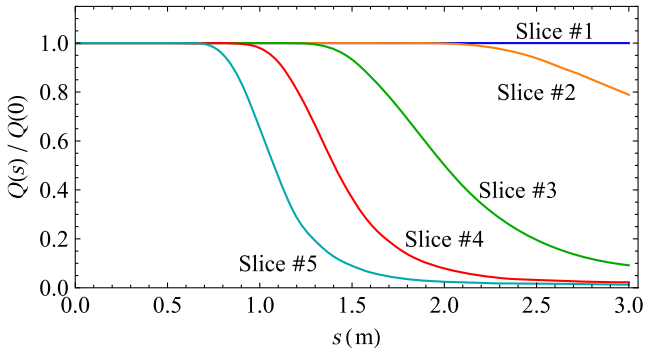

FIG. 15. Bunch charge in five longitudinal slices (shown in Fig. 8) as a function of propagation distance through the structure. The beam is initially offset vertically by $y_0 = 50$ μm. F_x is included.

quadrupole fields with alternating structures as described above may become impractical.

VI. CONCLUSIONS

In conclusion, we have experimentally studied the transverse effects of elliptical beams propagating through planar dielectric wakefield accelerating (DWA) structure with parameters mimicking future practical accelerating modules, i.e., gaps of a few millimeters, length of 200 mm, and beam offsets that are indicative of development of the beam breakup instability. Computer simulations match closely with the experimental data. As in [23], we observed a significant reduction of the transverse wakefields at the expense of some reduction in longitudinal fields with the increasing beam ellipticity. An important observation is that the suppression of the transverse wakefields becomes stronger while the beam moves closer to the dielectric plate, facilitating the overall suppression of the BBU instability. This experimental study has highlighted the importance of counteracting the quadrupole-like focusing wakefields that decrease the initial beam width thus diminishing the effect of the high beam aspect ratio.

To evaluate the feasibility of the elliptical beams concept with a practical DWA parameter range, simulations were conducted for an electron bunch having a 10-nC charge and 500-μm beam width propagating through the planar structure with a 2-mm gap. The simulations showed that defocusing quadrupole wakefields cause the onset of beam losses after 1 m of propagation and about half of the bunch charge is lost after 3 m.

To negate both focusing and defocusing wakefields, a sequence of the orthogonally oriented planar DWA structures has been proposed [32,35] and applied in energy dechirpers for FELs [25,33,34]. These studies, however, were conducted with small size circular beams. Practical realization of this concept with elliptical beams—even with a modest 500 μm width—is not trivial and may suffer from strong nonlinearities and significant wakefields strength at the edges of the beam in every other section of the structure. Simulations also demonstrated that this beam width is not sufficient to effectively suppress the development of the BBU instability. Further increase in the beam width would make transverse beam dynamics even more complicated and can prevent stable beam propagation in orthogonally oriented structures. The feasibility of this concept is the subject of further dedicated study.

ACKNOWLEDGMENTS

The authors acknowledge the support of the wider CLARA facility project team and the Cockcroft Institute core grant (STFC Grant No. ST/P002056/1) for funding part of this work.

[1] B. O'Shea, G. Andonian, S. Barber, K. Fitzmorris, S. Hakimi, J. Harrison, P. Hoang, M. Hogan, B. Naranjo, O. Williams *et al.*, Observation of acceleration and deceleration in gigaelectron-volt-per-metre gradient dielectric wakefield accelerators, Nat. Commun. **7**, 12763 (2016).

[2] A. Smirnov *et al.*, Development of a compact insertion device for coherent sub-mm generation, in *Proceedings of the 4th International Particle Accelerator Conference, IPAC-2013, Shanghai, 6 China, 2013* (JACoW, Shanghai, China, 2013), pp. 2295–2297.

[3] K. Bane, G. Stupakov, S. Antipov, M. Fedurin, K. Kusche, C. Swinson, and D. Xiang, Measurements of terahertz radiation generated using a metallic, corrugated pipe, Nucl. Instrum. Methods Phys. Res., Sect. A **844**, 121 (2017).

[4] A. Smirnov, R. Agustsson, W. Berg, S. Boucher, J. Dooling, T. Campese, Y. Chen, L. Erwin, B. Jacobson, J. Hartzell *et al.*, Observation of a variable sub-THz radiation driven by a low energy electron beam from a thermionic rf electron gun, Phys. Rev. ST Accel. Beams **18**, 090703 (2015).

[5] S. S. Baturin and A. Zholents, Upper limit for the accelerating gradient in the collinear wakefield accelerator as a function of the transformer ratio, Phys. Rev. Accel. Beams **20**, 061302 (2017).

[6] K. L. Bane, P. Chen, and P. B. Wilson, On collinear wakefield acceleration, IEEE Trans. Nucl. Sci. **32**, 3524 (1985).

[7] W. H. Tan, P. Piot, and A. Zholents, Formation of temporally shaped electron bunches for beam-driven collinear wakefield accelerators, Phys. Rev. Accel. Beams **24**, 051303 (2021).

[8] V. E. Balakin, A. V. Novokhatsky, and V. P. Smirnov, VLEPP: Transverse beam dynamics, Conf. Proc. C **830811**, 119 (1983), https://inspirehep.net/literature/198113.

[9] C. Li, W. Gai, C. Jing, J. G. Power, C. X. Tang, and A. Zholents, High gradient limits due to single bunch beam breakup in a collinear dielectric wakefield accelerator, Phys. Rev. ST Accel. Beams **17**, 091302 (2014).

[10] S. S. Baturin and A. Zholents, Stability condition for the drive bunch in a collinear wakefield accelerator, Phys. Rev. Accel. Beams **21**, 031301 (2018).

[11] A. Zholents, W. Gai, S. Doran, R. Lindberg, J. Power, N. Strelnikov, Y. Sun, E. Trakhtenberg, I. Vasserman, C. Jing *et al.*, A preliminary design of the collinear dielectric wakefield accelerator, Nucl. Instrum. Methods Phys. Res., Sect. A **829**, 190 (2016).

[12] D. Y. Shchegolkov, E. I. Simakov, and A. A. Zholents, Towards a practical multi-meter long dielectric wakefield accelerator: Problems and solutions, IEEE Trans. Nucl. Sci. **63**, 804 (2016).

[13] A. Tremaine, J. Rosenzweig, and P. Schoessow, Electromagnetic wake fields and beam stability in slab-symmetric dielectric structures, Phys. Rev. E **56**, 7204 (1997).

[14] S. S. Baturin, G. Andonian, and J. B. Rosenzweig, Analytical treatment of the wakefields driven by transversely shaped beams in a planar slow-wave structure, Phys. Rev. Accel. Beams **21**, 121302 (2018).

[15] T. Overton, T. Pacey, Y. Saveliev, and G. Xia, A stable drive beam for dielectric wakefield acceleration, in *Proceedings of the 12th International Particle Accelerator Conference, IPAC-2021, Campinas, Brazil, 2021* (JACoW, Geneva, Switzerland, 2021), pp. 528–531.

[16] S. Antipov, C. Jing, A. Kanareykin, J. Butler, V. Yakimenko, M. Fedurin, K. Kusche, and W. Gai, Experimental demonstration of wakefield effects in a THz planar diamond accelerating structure, Appl. Phys. Lett. **100**, 132910 (2012).

[17] G. Andonian, D. Stratakis, M. Babzien, S. Barber, M. Fedurin, E. Hemsing, K. Kusche, P. Muggli, B. OShea, X. Wei, O. Williams, V. Yakimenko, and J. B. Rosenzweig, Dielectric Wakefield Acceleration of a Relativistic Electron Beam in a Slab-Symmetric Dielectric Lined Waveguide, Phys. Rev. Lett. **108**, 244801 (2012).

[18] P. Emma, M. Venturini, K. L. F. Bane, G. Stupakov, H. Kang, M. Chae, J. Hong, C. Min, H. Yang, T. Ha, W. Lee, C. Park, S. Park, and I. Ko, Experimental Demonstration of Energy-Chirp Control in Relativistic Electron Bunches Using a Corrugated Pipe, Phys. Rev. Lett. **112**, 034801 (2014).

[19] Q. Gao, G. Ha, C. Jing, S. Antipov, J. Power, M. Conde, W. Gai, H. Chen, J. Shi, E. Wisniewski, D. Doran, W. Liu, C. Whiteford, A. Zholents, P. Piot, and S. S. Baturin, Observation of High Transformer Ratio of Shaped Bunch Generated by an Emittance-Exchange Beam Line, Phys. Rev. Lett. **120**, 114801 (2018).

[20] T. H. Pacey, Y. Saveliev, A. Healy, P. G. Huggard, B. Alderman, P. Karataev, K. Fedorov, and G. Xia, Continuously tunable narrow-band terahertz generation with a dielectric lined waveguide driven by short electron bunches, Phys. Rev. Accel. Beams **22**, 091302 (2019).

[21] J. Zemella, K. Bane, A. Fisher, M. Guetg, Z. Huang, R. Iverson, P. Krejcik, A. Lutman, T. Maxwell, A. Novokhatski, G. Stupakov, Z. Zhang, M. Harrison, and M. Ruelas, Measurements of wake-induced electron beam deflection in a dechirper at the linac coherent light source, Phys. Rev. Accel. Beams **20**, 104403 (2017).

[22] A. Novokhatski, D. Bohler, A. Brachmann, W. Colocho, F.-J. Decker, A. S. Fisher, M. Guetg, R. Iverson, P. Krejcik, J. Krzywinski *et al.*, A simple method for a very short x-ray pulse production and attosecond diagnostic at LCLS, Nucl. Instrum. Methods Phys. Res., Sect. A **921**, 57 (2019).

[23] B. D. O'Shea, G. Andonian, S. S. Baturin, C. I. Clarke, P. D. Hoang, M. J. Hogan, B. Naranjo, O. B. Williams, V. Yakimenko, and J. B. Rosenzweig, Suppression of Deflecting Forces in Planar-Symmetric Dielectric Wakefield Accelerating Structures with Elliptical Bunches, Phys. Rev. Lett. **124**, 104801 (2020).

[24] D. Angal-Kalinin *et al.*, Design, specifications, and first beam measurements of the compact linear accelerator for research and applications front end, Phys. Rev. Accel. Beams **23**, 044801 (2020).

[25] M. Colling, D. Dunning, B. Fell, T. Pacey, and Y. Saveliev, Mechanical design of a dielectric wakefield dechirper system for CLARA, in *Proceedings of the 10th International Particle Accelerator Conference, IPAC'19, Melbourne, Australia, 2019* (JACoW, Geneva, Switzerland, 2019), pp. 1912–1915.

[26] T. Pacey, D. Dunning, Y. Saveliev, and G. Xia, Phase space manipulation of sub-picosecond electron bunches using dielectric wakefield structures, in *Proceedings of the 8th International Particle Accelerator Conference, IPAC-2017, Copenhagen, Denmark, 2017* (JACoW, Geneva, Switzerland, 2017), pp. 3302–3304.

[27] M. Rosing and W. Gai, Longitudinal- and transverse-wakefield effects in dielectric structures, Phys. Rev. D **42**, 1829 (1990).

[28] S. Bettoni, P. Craievich, A. A. Lutman, and M. Pedrozzi, Temporal profile measurements of relativistic electron bunch based on wakefield generation, Phys. Rev. Accel. Beams **19**, 021304 (2016).

[29] S. S. Baturin, I. L. Sheinman, A. M. Altmark, and A. D. Kanareykin, Transverse operator method for wakefields in a rectangular dielectric loaded accelerating structure, Phys. Rev. ST Accel. Beams **16**, 051302 (2013).

[30] P. Craievich and A. A. Lutman, Effects of the quadrupole wakefields in a passive streaker, Nucl. Instrum. Methods Phys. Res., Sect. A **865**, 55 (2017).

[31] P. Piot, C. Behrens, C. Gerth, M. Dohlus, F. Lemery, D. Mihalcea, P. Stoltz, and M. Vogt, Generation and Characterization of Electron Bunches with Ramped Current Profiles in a Dual-Frequency Superconducting Linear Accelerator, Phys. Rev. Lett. **108**, 034801 (2012).

[32] L. Xiao, W. Gai, and X. Sun, Field analysis of a dielectric-loaded rectangular waveguide accelerating structure, Phys. Rev. E **65**, 016505 (2001).

[33] M. Guetg *et al.*, Commissioning of the RadiaBeam/SLAC dechirper, in *Proceedings of the 7th International Particle Accelerator Conference, IPAC-2016, Busan, Korea, 2016* (JACoW, Geneva, Switzerland, 2016), pp. 809–812.

[34] Y.-W. Gong, M. Zhang, W.-J. Fan, D. Gu, and M.-H. Zhao, Beam performance of the SHINE dechirper, Nucl. Sci. Tech. **32**, 29 (2021).

[35] W. Lynn, G. Andonian, N. Majernik, and J. Rosenzweig, Strong quadrupole wakefield based focusing in dielectric wakefield accelerators, in *Proceedings of the 12th International Particle Accelerator Conference, IPAC-2021, Campinas, Brazil, 2021* (JACoW, Geneva, Switzerland, 2021), pp. 4059–4061.